Atomistic study of xenon crystal growth via low-temperature atom beam deposition

Nicola Totò,* Christian Schön,† and M. Jansen‡
Max Planck Institute for Solid State Research, Heisenbergstrasse 1, 70569 Stuttgart, Germany
(Received 3 March 2010; revised manuscript received 16 July 2010; published 1 September 2010)

We studied theoretically the deposition of Xe atoms on a sapphire substrate and the subsequent growth of ordered Xe phases via the low-temperature atom beam deposition method. This chemical synthesis method [D. Fischer and M. Jansen, J. Am. Chem. Soc. **41**, 1755 (2002)] is particularly suitable for synthesizing metastable solid compounds. The modeling procedure consisted of several steps, where we used empirical potentials to model the interactions within the substrate, the Xe-Xe interactions in the gas phase and the solid, and the interactions between the Xe atoms and the substrate. In a first step, we established that under the experimental conditions, no Xe clusters formed in the gas phase, and thus the deposition could be described by the adsorption of single Xe atoms on the substrate at low temperatures. Next, we simulated the Xe deposition process and we studied the growth mode depending on various synthesis parameters such as the deposition rate and the temperature of the substrate. Finally, the deposited Xe layers were tempered and the structure of the resulting compound was analyzed. We studied the establishment of locally ordered regions as a function of time, both during the deposition and the tempering. We observed that the final configuration was always crystalline, although defects such as stacking faults and dislocations were likely to form. The occurrence of different growth modes and the formation of defects were explained by studying diffusion and adsorption processes on the surface of both the substrate and the depositing phase.

DOI: 10.1103/PhysRevB.82.115401 PACS number(s): 81.15.Np, 81.15.Aa, 83.10.Rs, 68.55.−a

I. INTRODUCTION

Growth processes of solid materials are of great interest from both the fundamental and the technological point of view. Understanding how different growth procedures lead to different polymorphs of the same substance, for instance, is a key issue in natural sciences with many applications in fields as diverse as the electronic, the chemical, and the pharmaceutical industry. Since different modifications of the same material display in general different properties,[1] it is of extreme importance to study the relationship between the synthesis route followed and the resulting modification and morphology of the grown compound.

Although recent progress has made available tools for the microscopy and spectroscopy of solid compounds during the whole growth process,[2–4] atomistic simulations prove invaluable in casting light on the mechanisms which determine the growth mode.[5,6] In particular, molecular dynamics (MD) has been extensively used to study growth processes of materials from both the liquid and the gas phase,[7–14] especially in an attempt to model the experimental conditions occurring during a molecular-beam epitaxy experiment.[15]

Recently, a solid-state synthesis technique, called the low-temperature atom beam deposition method, has been developed and used to produce stable and metastable phases of oxide,[16] nitride,[17] and halide compounds,[18,19] some of which had never been accessible before using any alternative synthesis route. During low-temperature atom beam deposition, the metal constituents of the desired compound are initially evaporated using thermal effusion cells. Simultaneously, the oxygen molecules, for example, are broken up to form a low-density atomic gas. The oxygen-metal gas thus produced is then deposited on a cold substrate, which is maintained at liquid-nitrogen or liquid-helium temperature. X-ray amorphous deposits are obtained as a result of this procedure. Finally, upon slow heating, crystals of various stable and metastable modifications are generated.

Understanding this procedure is of high scientific and technological interest, due to its unusually high degree of control over the synthesis parameters as compared to most other solid-state synthesis methods. The goal of this study is thus to model such a synthesis throughout all its stages.

As an example system, we have chosen the deposition of xenon on a sapphire (Al_2O_3) substrate, followed by a tempering stage at various temperatures. Such an experiment has recently been performed and preliminary results indicate that both fcc and hcp Xe crystals have formed.[20]

Xe displays extremely low reactivity, relatively high atomic mass, and high polarizability. Thanks to these properties, solid Xe is commonly used as an inert matrix in which single atoms, molecules, or atom clusters are trapped in order to study their optical properties.[21,22] Furthermore, Xe films have recently been used as buffer layers during metal cluster deposition in order to screen the cluster from the interaction with the substrate.[23,24] Therefore, being able to control which structure and microstructure form, as well as what kind of defects are present, is important also for applications such as those mentioned above.

In this work, we report on an atomistic study of growth of solid Xe by deposition from the gas phase. In the first stage, we have studied the dynamics of the Xe atoms in the gas phase prior to adsorption. Subsequently, we modeled the impact of the gas-phase atoms on the substrate surface, as well as their adsorption and diffusion, which lead to the formation of solid Xe. Finally, we have investigated the effect of tempering and annealing the system obtained as a result of the deposition, with a particular focus on identifying the formation of different Xe modifications and the generation of defects.

TABLE I. Parameters of the Matsui potential.

	q ($\|e\|$)	A (Å)	B (Å)	C (Å^3 kJ$^{1/2}$ mol$^{-1/2}$)
Al	1.4175	0.7852	0.034	36.82
O	−0.9450	1.8215	0.128	90.61

II. MODEL AND CALCULATION METHODS

All calculations were performed by using classical MD. The Newtonian equations of motion were solved by means of the Velocity-Verlet algorithm.[25] Time steps used were in the range between 2 and 6×10^{-15} s.

Simulations of deposition and tempering were carried out within a rectangular prismatic simulation unit cell. The system was comprised of the Al_2O_3 substrate and the depositing Xe species. The axes were oriented in such a way that the substrate surface lay in the xy plane and the vertical direction was parallel to the z axis. The top substrate surface had vertical z coordinate equal to 0.

A. Potentials

The potential chosen to describe atomic interactions in Al_2O_3 was the Matsui potential,[26] already successfully used in previous studies.[27,28] The Matsui potential is a sum of pairwise terms of the form,

$$V(r_{ij}) = \frac{q_i q_j}{r_{ij}} - \frac{C_i Cj}{r_{ij}^6} + D(B_i + B_j)\exp\left(\frac{A_i + A_j - r_{ij}}{B_i + B_j}\right), \quad (1)$$

where the first term describes the Coulomb interaction, the second the van der Waals interaction, and the third is the repulsive term. In Eq. (1), r_{ij} is the distance between particle i and j, and D is a force constant which is equal to 4.184 kJ Å^{-1} mol^{-1}. The remaining free parameters are listed in Table I.[26]

Due to the two-dimensional periodicity of the system, a treatment of the Coulomb term in the Matsui potential within the Ewald scheme would have been cumbersome and computationally expensive. Therefore, we opted for the damping procedure proposed by Wolf *et al.*,[29] which has the advantage of being applicable to systems with arbitrary geometry, without introducing a significant error into the potential calculation. We used a damping factor of 0.27 Å^{-1} and we cut off the potential at 10 Å.

Atomistic interactions between Xe atoms were modeled via the Lennard-Jones 12-6 potential. The parameters we used for the energy well depth $\varepsilon_{\text{Xe-Xe}}$ and the typical interatomic distance $\sigma_{\text{Xe-Xe}}$ were 0.021 eV and 4.0 Å, respectively.[30,31]

The interactions between Xe atoms and the Al and O atoms constituting the substrate were then described by a modified Lennard-Jones potential type of the form,

$$V_{Y\text{-Xe}}(r_{ij}) = 4\varepsilon_{Y\text{-Xe}}\left[\left(\frac{\sigma_{Y\text{-Xe}}}{r_{ij}}\right)^{10} - \left(\frac{\sigma_{Y\text{-Xe}}}{r_{ij}}\right)^{5}\right], \quad (2)$$

where Y stands for either Al or O. Here the long-range attractive term varies as the inverse fifth power of the distance between a pair of particles.

The dependence of the potential on the inverse fifth power of the distance was chosen to account for the average effect of the many contributions making up the total interaction between a Xe atom and the substrate. It was assumed that, in a first approximation, each substrate ion interacting with the Xe atom induces a dipole on the latter. However, these dipoles are oriented in different manners, depending on the charge and the position of the inducing ion. Thus, the induced dipole contribution due to, e.g., an Al ion is partly compensated by that due to a neighboring O ion, essentially resulting in an effective three-body interaction. Since the Al_2O_3 surface consists of neighboring Al cations and O anions whose separation (1.7 Å) is small compared to the spatial extension of a Xe atom (about 4.5 Å), the Xe atom close to the surface experiences an averaged potential resulting from the interaction with many ions located at nearly the same distance. Furthermore, the ions cannot be simply approximated as point charges, as their polarizable electron shells also interact with the Xe atoms, particularly at short Xe-ion distances. As a consequence, the net effect of this multi-ion contribution is better approximated by a dipole-induced-dipole type of interaction, scaling as the inverse fifth power of the distance, rather than by a sum of point-charge-induced-dipole interaction terms.

For the Al-Xe and the O-Xe interactions, the location of the minimum of the potential well, on which the parameter σ depends, was chosen to be equal to the sum of the ionic radius of the cation (0.675 Å) or of the anion (1.26 Å), and the van der Waals radius of Xe (2.16 Å). This gave values of 2.468 Å and 2.977 Å for $\sigma_{\text{Al-Xe}}$ and $\sigma_{\text{O-Xe}}$, respectively.

The depth $\varepsilon_{\text{Al-Xe}}=\varepsilon_{\text{O-Xe}}=\varepsilon_{\text{Al}_2\text{O}_3\text{-Xe}}$ of the potential well was assumed to be the same for both the Al-Xe and the O-Xe interactions. In order to determine the value of this parameter, the energy of a single Xe atom adsorbed on the relaxed surface was calculated as a function of $\varepsilon_{\text{Al}_2\text{O}_3\text{-Xe}}$. For each value of $\varepsilon_{\text{Al}_2\text{O}_3\text{-Xe}}$, the adatom was placed at several locations on the surface and the system was then relaxed to the local energy minimum. The adsorption energy was finally obtained as the difference between the energy of the relaxed system in the presence and in the absence of the adsorbate, respectively. Figure 1 shows the results for the calculations of the adsorption energy, which was found to vary linearly with respect to the potential parameter $\varepsilon_{\text{Al}_2\text{O}_3\text{-Xe}}$.

The value of $\varepsilon_{\text{Al}_2\text{O}_3\text{-Xe}}$ chosen was 0.015 eV, which gave an adsorption energy of 0.133 eV. This matched well with the values reported in the literature for the adsorption energy of Xe on ionic surfaces, varying between about 0.12 and 0.18 eV.[32] Table II summarizes the values of the potential parameters modeling interactions between two Xe atoms, a Xe atom and an Al cation, and a Xe atom and an O anion. The Xe-Xe, Al-Xe, and O-Xe potentials were cut off at a distance of 10 Å, 6.5 Å, and 7.8 Å, respectively, and smoothly brought to zero by means of a fifth-order polynomial.

B. Model of substrate

The substrate was an Al_2O_3 slab chosen in such a way as to expose the O-terminated (0001) surface. Although the Al-terminated surface had been previously calculated to be more

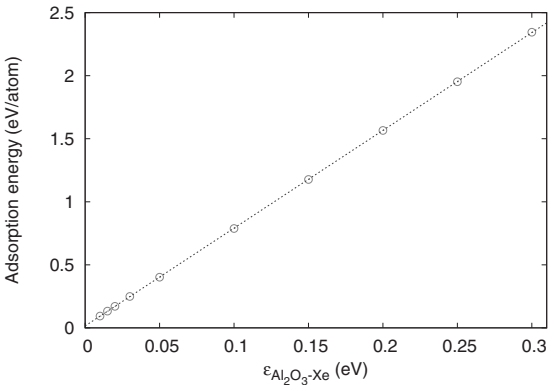

FIG. 1. Energy of adsorption of a Xe atom on the Al_2O_3 surface as a function of the strength $\varepsilon_{Al_2O_3\text{-}Xe}$ of the interaction between the substrate and a Xe particle. The dotted line is a linear fit to the calculated data.

stable than the O-terminated (0001) surface,[33] we still decided to use the latter in order to reproduce more closely the experimental conditions. Given that the pressure in the chamber before the deposition started was of around 10^{-8} mbar and that the substrate was not treated with any cleaning process,[20] we expected the exposed Al layer to be passivated with O and other species present in the chamber within a few seconds. Therefore, it was reasonable to assume an O-terminated surface as a starting configuration before deposition was initiated.

The initial slab was comprised of 3600 atoms and was obtained by constructing an *ABA* stacking of close-packed planes of O atoms. Six close-packed planes made of 360 oxygen atoms and with lateral dimensions of 50.4 Å $\times$48.5 Å were used. The nearest-neighbor distance between O atoms was 2.8 Å. Two thirds of the octahedral hollow sites between two adjacent close-packed O planes were filled with Al atoms, in such a way as to mimic the corundum crystal structure. In the course of the simulation, the bottom O and Al planes were kept fixed, in order to reproduce the stabilizing effect of the bulk crystal.

The initial slab was then locally minimized by using an MD-assisted quenching procedure. At each MD iteration, after solving the classical equations of motion via the Velocity-Verlet algorithm, the quenching was accomplished by canceling all those components of an atom's velocity whose scalar product with the force acting on the atom was negative. Periodic boundary conditions across the plane parallel to the O planes (*xy* plane) were applied. Upon quenching, the topmost O plane was observed to relax inward, in such a way as to reduce the surface dipole moment.

TABLE II. Parameters of the Lennard-Jones potential used for interaction between Xe atoms, and of the 10-5 potential used for interactions between substrate and Xe atoms.

System	$\sigma_{X\text{-}Y}$ (Å)	$\varepsilon_{X\text{-}Y}$ (eV)
Xe-Xe	4.0	0.021
Al-Xe	2.468	0.015
O-Xe	2.977	0.015

Before initiating the actual deposition, the minimized slab was equilibrated by performing MD for a time interval of around 1 ps at the temperature of the deposition. A simple thermostat based on velocity rescaling was used and applied to all atoms lying within a distance less than one third of the slab height from the bottom of the slab. The equilibrated structure was then used as the substrate for the deposition and growth simulation.

C. Properties of the Xe gas phase and modeling of the deposition stream

As a preliminary study, we modeled the dynamics of Xe in the gas phase over a wide range of pressures (10^{-7}–10^{3} bar). A rectangular prismatic simulation box was used and periodic boundary conditions were applied in all three orthogonal directions. The temperature was kept constant by means of an Andersen's thermostat,[34] whose frequency was chosen between 10^{11} and 10^{12} s^{-1}/particle. The Andersen thermostat has been successfully used in nucleation studies[35] and its performance has proved extremely satisfactory as compared with that of other thermostatting methods.[36]

At the beginning of the simulation, Xe atoms were made to occupy the nodes of a grid. The grid spacing, and therefore the gas density, were determined in such a way that the gas was at the desired pressure given the thermostat temperature, according to the ideal gas law.

We then performed MD in the (NVT) ensemble. In order to identify the Xe clusters that remained stable for a certain time interval, we used a bond-network algorithm which associated each atom with a cluster based on the list of nearest neighbors of that atom. Two Xe atoms were considered neighbors if they were less than $1.5\sigma_{Xe\text{-}Xe}$ apart. It was found that, within a wide range of temperatures from 50 to 500 K, no stable cluster could form for all pressures less than about 10 bar.

In the experiment, the pressure in the vacuum chamber during deposition was about 10^{-5} mbar.[20] Therefore, we could safely rule out any possibility of cluster formation in the gas phase and assume that, during deposition, single Xe atoms impinged onto the growing sample.

Based on these results, we implemented a model of the deposition process, where Xe particles were deposited one by one at a given frequency with a predefined initial kinetic energy. The initial kinetic energy chosen for depositing adatoms was in the range 0.01–0.03 eV, corresponding to thermal deposition. The initial velocity was directed along the *z* axis and oriented toward the substrate surface. The initial distance of the particle from the growing surface was fixed and set to a typical value of about 10 Å. The lateral position of the impinging atom was randomly chosen. The surface of the Al_2O_3 substrate was located at $z=0$. The bottom part of the surface slab was kept fixed and a thermostat was applied, as described in Sec. II B. Periodic boundary conditions across the horizontal *xy* plane were imposed.

The temperature was monitored during the course of the simulation. The system was divided into slices parallel to the *xy* plane and the average temperature of the atoms contained

in each slice was calculated by using the kinetic definition of temperature. The slice thickness was chosen in the range of about 2–4 Å, thus guaranteeing that on the order of 100 particles were contained in each slice.

D. Bond angle analysis

Several methods have been developed in the past few decades to study the emergence of ordered structures in amorphous systems such as liquids and glasses in the regime of undercooling.[37–41] For our purpose of identifying regions with crystalline structure within the deposited species, we worked out a simple procedure based on the distribution of bond angles between an atom and its nearest neighbors.

First of all, given a Xe atom in the structure, we defined its nearest neighbors as those other Xe atoms whose position lay within a sphere having the former particle as a center and a radius of $1.15r_0$, where r_0 is the minimum of the Lennard-Jones potential well. This gave a maximum distance for two neighboring Xe atoms of about 5.16 Å. We verified that this value made sense by calculating the radial distribution function of bulk Xe in the temperature range of concern. In all cases, the radial distribution function vanished, after the first peak, within the distance interval from 5.2 to 5.6 Å. Therefore, 5.2 Å could be considered as the cut-off value for the first neighbor distance.

After associating each Xe atom with a list of nearest neighbors, we selected only 12-fold-coordinated atoms, since we were interested in possible crystalline order in the deposited Xe. Given one selected atom, the angle formed by the triplet consisting of the atom itself in the vertex and each couple of its nearest neighbors was calculated. In this way, each atom was associated with a bond angle distribution. Subsequently, the bond angle distribution of each atom was compared to that of an atom in an ideal fcc and hcp crystal. A χ^2 test was then performed in order to decide whether the environment around the atom belonged to one of the two ideal close-packed types or whether it was to some extent distorted. In case the *error* resulting from the test was too high, the atom was labeled as of unidentified type.

III. RESULTS

A. Deposition at high rate

1. Deposition process

We first simulated deposition at a rate of 2×10^{11} atoms/s, which corresponded to a growth rate of about 10^9 monolayers/s. This is obviously much faster than in the experiment, where growth rates of about 1 monolayer/s were typically chosen.[20]

The structures grown at this rate were all completely amorphous and did not display any degree of order. In no case was intermixing of substrate and growing species observed. An example of such a structure, grown with a substrate temperature of 50 K, is shown in Fig. 2(a). Regardless of the substrate temperature, the temperature of the deposited layers was observed to fluctuate around 200 K (see Fig. 3). The only difference between different substrate temperatures was the fluctuation amplitude with larger fluctuations occurring for higher temperatures.

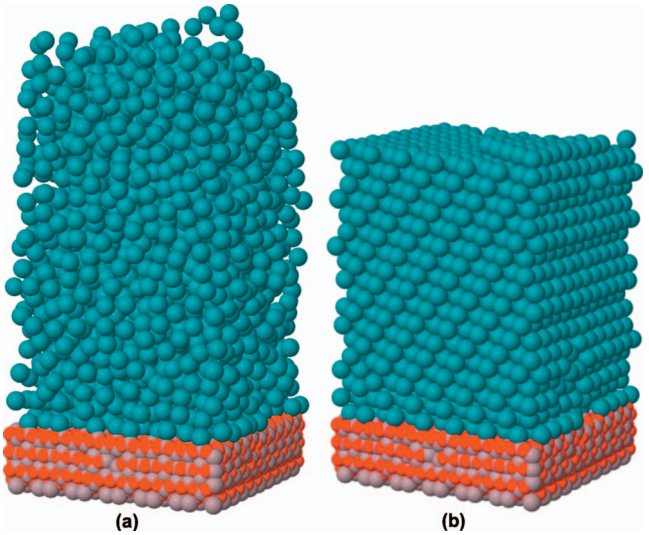

FIG. 2. (Color) (a) Example of a structure obtained after depositing single Xe atoms with a rate of 2×10^{11} atoms/s on an Al_2O_3 substrate maintained at a temperature of 50 K. The snapshot was taken after 12 ns from the beginning of the deposition. (b) Configuration obtained by tempering the structure in panel (a) at 10 K for 60 ns. Blue, gray, and red spheres represent Xe, O, and Al atoms, respectively.

2. Tempering of structures grown at high rate

After growing the amorphous structures as described above, we tempered them at several temperatures in the range between 10 and 150 K, by applying the thermostat to the lower part of the substrate. We observed that for all annealing temperatures investigated, the amorphous structure obtained as a result of the deposition process underwent a phase transition toward a more ordered configuration. The transition from amorphous to crystalline states started with

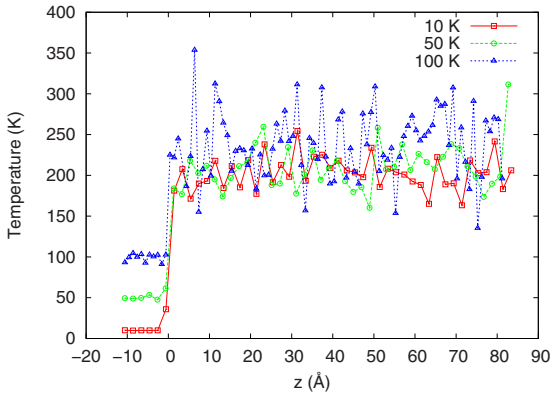

FIG. 3. (Color online) Temperature as a function of the height along the z direction normal to the surface of structures obtained by depositing Xe at a rate of 2×10^{11} atoms/s with the substrate maintained at a temperature of 10, 50, and 100 K. The surface of the substrate lay on the plane $z=0$. The temperature was measured on substrates obtained after 4 ns from the beginning of the deposition.

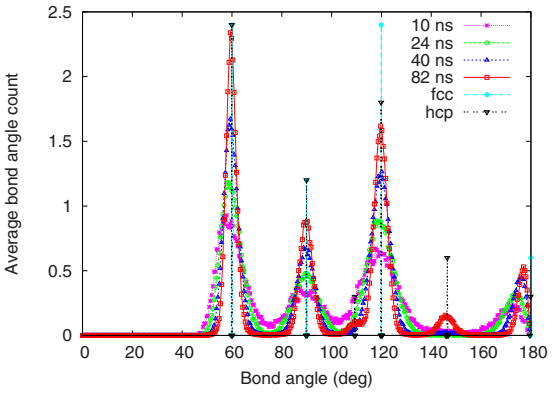

FIG. 4. (Color online) Bond angle distribution averaged over all 12-fold-coordinated Xe atoms of a hot sample tempered at 25 K at four consecutive time instants during the process. Corresponding bond angle distribution for an ideal fcc and hcp lattice are also shown for comparison. For clarity of display, these two latter distributions were divided by a factor of 10.

the formation of 12-fold-coordinated nuclei before the Xe temperature decreased down to the substrate temperature. Eventually, the temperature of the whole sample was uniform and the system reached local equilibrium. The final stage of the process was a transition to fcc or hcp packing. Figure 2(b) shows, as a typical example, a structure obtained by tempering a hot sample at a temperature of 10 K for 60 ns.

By performing the bond angle analysis during the cooling process, it was possible to observe the emergence of long-range ordering in the initially amorphous sample. In Fig. 4 the average bond angle distribution calculated at several instants during tempering at 25 K of an initially hot sample is plotted. The bond angle distribution for a perfect fcc and hcp crystal, respectively, are also displayed in the same graph. The whole process is made visible in Fig. 5, where the results of the bond angle analysis are shown for the structure snapshots taken at the same instants as in Fig. 4. One can observe the formation of some initial ordered clusters with fcc-like packing, their extending throughout the whole sample, and finally some areas of hcp-like packing appearing and spreading across the sample.

In this way, we could follow the process of crystallization from the amorphous phase in all its stages. Typically, after the temperature had decreased down to approximately 130 K, the atoms started arranging themselves such that they gained 12-fold coordination. These 12-fold-coordinated nuclei formed initially in proximity to the substrate surface [Fig. 5(a)]. As the deposit cooled further, the initial 12-fold-coordinated core extended to the whole Xe sample and atoms slowly arranged into a close-packed crystal structure displaying large regions with fcc or hcp stacking [Figs. 5(b)–5(d)].

In all cases, the structure was observed to thermalize into a crystalline close-packed phase. Point defects, dislocations, and stacking faults were frequently produced in the course of the tempering process. Dislocations appeared in all cases studied in approximately the same region of the sample at a distance of about 10 Å away from the substrate surface. The plane where the dislocation lay marked the boundary between the area without any specific crystalline order closer to the substrate, and the area with a distinctive close-packed crystal structure, be it fcc like or hcp like. Dislocations were probably produced by the stress experienced by the Xe atoms which were closest to the substrate and therefore were affected by both the substrate potential and the interaction with Xe atoms in the layers above.

We often also observed an alternation of fcc and hcp stackings giving rise to a series of stacking faults [Figs. 5(c) and 5(d)]. These stacking faults corresponded to close-packed planes in the crystal and were mostly found parallel to planes forming an angle of approximately 60° with the plane of the substrate surface. This was expected since the layers of adsorbed Xe parallel to the substrate surface were arranged in a close-packed fashion. In very few cases, stacking faults were obtained which lay on planes parallel to the substrate surface, an example of which is shown in Fig. 6(b).

Figure 6 shows some of the configurations obtained during tempering at several of the temperatures we studied. Typically, stacking faults were found to originate at the bottom of the deposited phase, at the interface with the substrate. This original seed of the stacking fault was then observed to propagate across the whole solid phase by growing upward across a close-packed plane. This mechanism is evident by comparing the configurations (c) and (d) of Fig. 5. Although not directly comparable, these results are consistent with the findings of a recent MD study where nucleation in a homogeneous Lennard-Jones liquid was investigated during moderate and deep undercooling.[42] When the liquid was moderately undercooled, a mixture of fcc- and hcp-like regions was observed, in a similar fashion to what we obtained in our simulations.

In order to speed up the process of heat transfer through the interface between the substrate and the grown species, the strength $\varepsilon_{Al_2O_3\text{-}Xe}$ of the interaction between a Xe atom and the substrate was increased by a factor of nearly 10 to the value of 0.1 eV. We verified that increasing this parameter resulted in the sample equilibrating to the thermostat temperature but in a much shorter time. Also in this case, the preferred type of packing turned out to be of fcc type, which was the equilibrium configuration most often found.

Stacking faults separating fcc and hcp areas also occurred, although at temperatures between about 5 and 40 K, a lower temperature range than in the previous case. Moreover, the stacking faults were always parallel to the plane of the substrate surface. Figure 7 shows the results of the bond angle analysis performed on configurations obtained after tempering the hot sample at different temperatures. In contrast to the previous case of low substrate-Xe interaction, stacking faults running along diagonal close-packed directions of the crystal were never obtained with the increased value of $\varepsilon_{Al_2O_3\text{-}Xe}$.

Overall, the results obtained in the two series of calculations with different values of $\varepsilon_{Al_2O_3\text{-}Xe}$, suggest that the stacking fault energy for this system is low and that the competition between fcc and hcp ordering is particularly strong. Furthermore, the strength of the interaction between substrate and deposited layers clearly influenced the generation of defects during the deposition and tempering process.

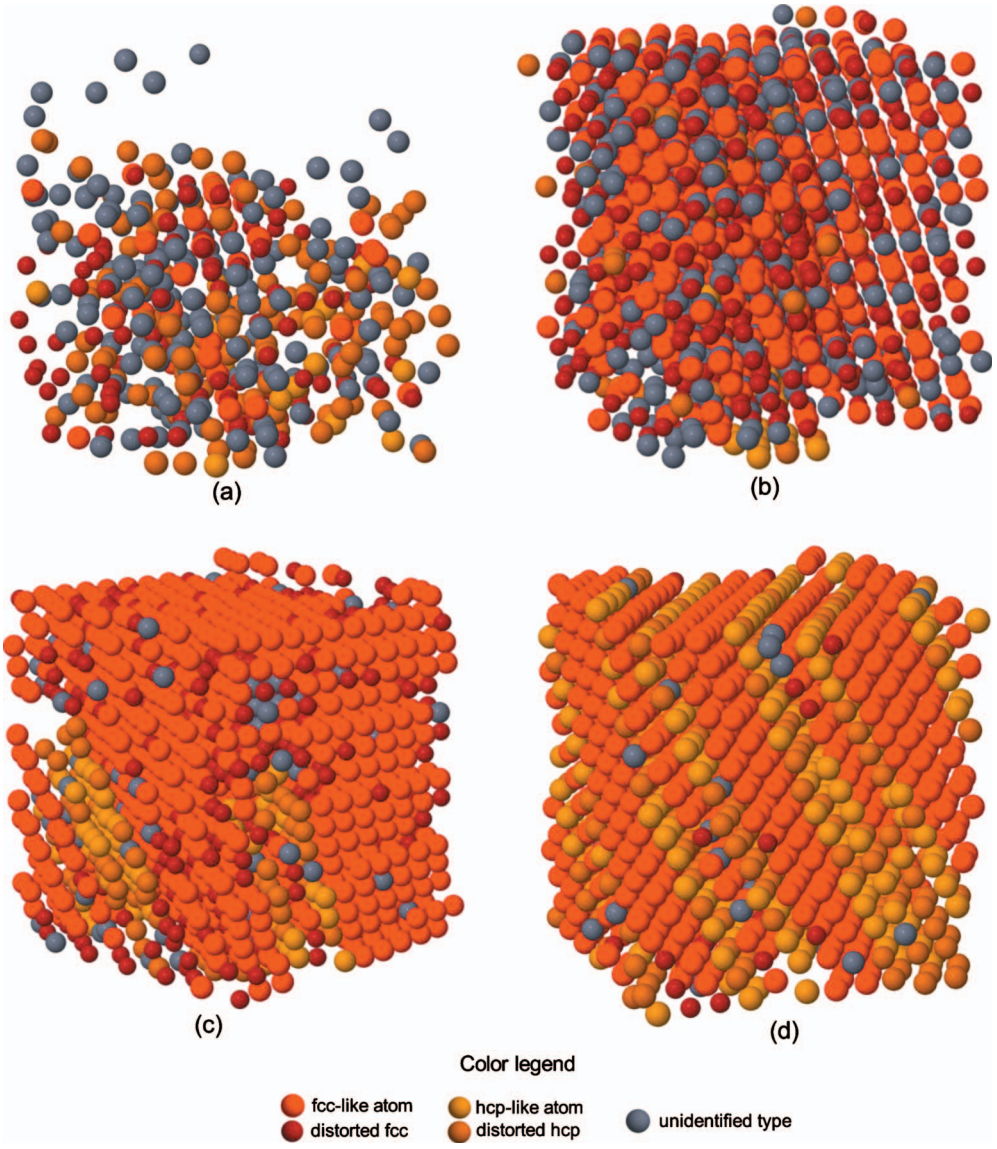

FIG. 5. (Color) Result of single atom bond angle analysis performed on successive instants during tempering at 25 K of a hot sample. The same structures were considered as those whose average bond angle distribution is plotted in Fig. 4. Only 12-fold-coordinated Xe atoms are shown. Simulation times are as follows: (a) 10 ns, (b) 24 ns, (c) 40 ns, and (d) 82 ns.

However, upon comparing structural quantities calculated in the cases studied, we verified that a few monolayers above the interface the deposited Xe was crystalline, close packed, and the lattice constant was the same, regardless of the value of $\varepsilon_{Al_2O_3\text{-}Xe}$ used.

B. Growth at lower rate

Simulations were also performed where the deposition rate was decreased to 10^{10} atoms/s, i.e., an order of magnitude lower than in the previous case. The substrate temperatures investigated varied within the range of 10–100 K.

Throughout the whole range of investigated temperatures, the grown structures displayed a high degree of order and turned out to be arranged in one of the two possible close-packed crystal structures. As an example, in Fig. 8 several stages of a simulated deposition process at a substrate temperature of 25 K are shown. The grown Xe assumed a close-packed crystal structure from the early stage of the deposition process, as seen from the radial distribution functions calculated for the configurations shown in Fig. 8 (see Fig. 9).

As the deposition continued, some surface roughness developed thus giving rise to three-dimensional islands. By performing the bond angle analysis (see lower panels of Fig. 8), it was possible to observe how several stacking faults originated at the beginning of the deposition in proximity to the substrate surface, and propagated subsequently across the growing sample along close-packed directions in the crystalline structure.

Structures obtained by depositing Xe atoms at different substrate temperatures were compared, and in all cases crystalline structures were obtained. The deposited phase temperature, monitored during the simulated growth, proved to be generally higher by about 20–30 K than that of the sub-

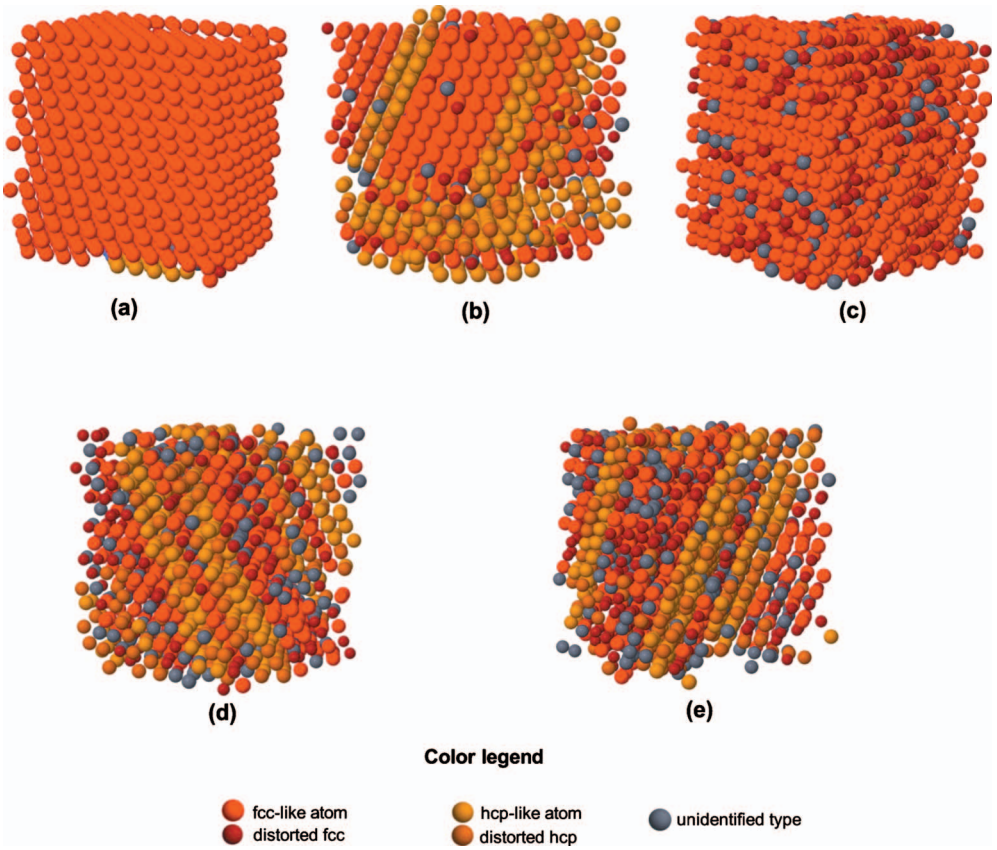

FIG. 6. (Color) Bond angle analysis performed on structures obtained as a result of tempering hot samples as obtained after a simulated deposition with a rate of 2×10^{11} atoms/s. Only 12-fold-coordinated Xe atoms are shown. Tempering temperatures and simulation times are as follows: (a) 10 K, 64 ns; (b) 25 K, 72 ns; (c) 50 K, 110 ns; (d) 75 K, 140 ns; and (e) 100 K, 56 ns.

strate (see Fig. 10). The roughness of the surface was found to decrease with increasing substrate temperature, from the value of 10 K, all the way up to 100 K, which was the maximum substrate temperature used. Figure 11 presents an overview of the structures grown at different temperatures.

In summary, by performing an analysis of the bond angle distribution and calculating the radial distribution function along the various stages of the depositions process (see Fig. 12), we were able to follow the emergence of long-range order in the grown species and observe the formation of defects in their making. In particular, we observed the formation of stacking faults in all structures obtained as a result of a simulated deposition at substrate temperatures lower than 70 K. Such an alternation of fcc- and hcp-like ordering was also in agreement with preliminary results of the experiment obtained by taking x-ray diffractograms of the deposited Xe on a Al_2O_3 substrate.[20] Above 75 K, the temperature of the grown species was too high to allow the structure to fully equilibrate into a properly crystalline ordered phase.

IV. DISCUSSION

All our calculations showed clearly that when Xe is deposited on an alumina substrate, it tends to assume a crystalline ordered phase for all substrate temperatures below the melting point of Xe. However, the presence of defects was observed on a regular basis. Notably, stacking fault alternations were often obtained in the deposited species, indicating a high degree of competition between fcc and hcp ordering.

In order to gain additional insight into various aspects of the deposition and the growth process, we investigated the difference in stability between bulk Xe displaying fcc and hcp packing (Sec. IV A). Next (Sec. IV B), we studied adsorption and several diffusion processes of a single Xe adatom on a Xe surface. These results were used to explain the temperature-induced transition we observed between three-dimensional and two-dimensional layer-by-layer growth. Finally (Sec. IV C), we used some of the results obtained in Secs. IV A and IV B to cast light on the origin of stacking fault formation in the deposited Xe sample.

A. Local optimization of close-packed crystal structures

In order to quantify the difference in stability between the fcc and hcp crystal structure, we locally minimized a slab consisting of stacked close-packed planes following both the *ABC* and the *ABA* packing. The initial slab was comprised of 1872 atoms. Periodic boundary conditions were applied on a prismatic box which fit the slab and whose dimensions were 50.400 Å, 43.648 Å, and 44.581 Å, in the x, y, and z directions, respectively, for a nearest-neighbor distance of 4.384 Å.

Initially, the lattice constant was varied, in an attempt to find the optimal interatomic distance in the crystal. It turned

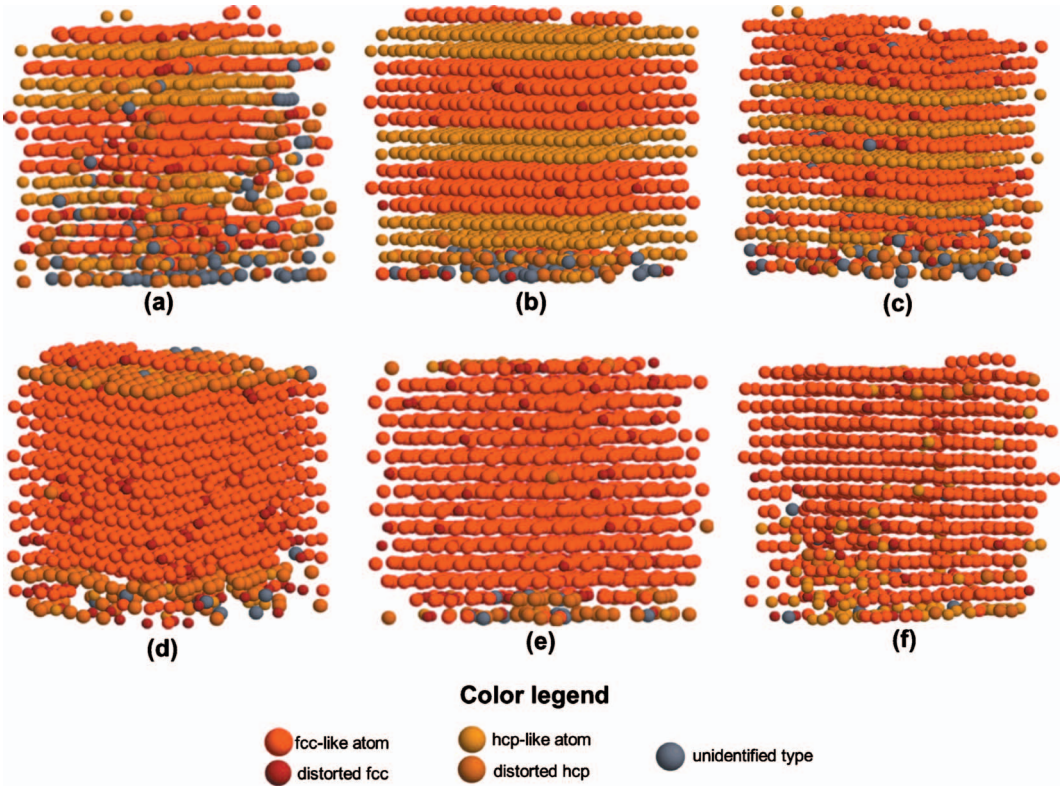

FIG. 7. (Color) Bond angle analysis performed on structures obtained as a result of tempering the same hot sample as obtained after a simulated deposition with a rate of 2×10^{11} atoms/s. The parameter $\varepsilon_{Al_2O_3\text{-}Xe}$ was increased to the value of 0.1 eV in order to speed up the equilibration process. Tempering temperature and simulation times are as follows: (a) 5 K, 4 ns; (b) 10 K, 4 ns; (c) 25 K, 4 ns; (d) 50 K, 8 ns; (e) 75 K, 4 ns; and (f) 100 K, 4 ns.

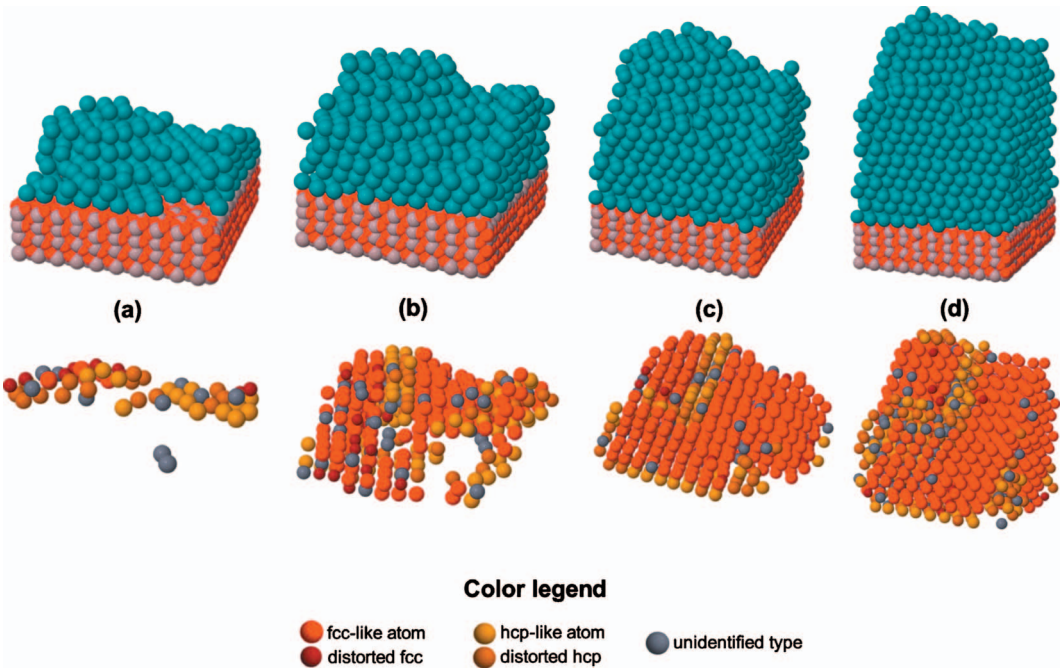

FIG. 8. (Color) Sequence of snapshots taken during a simulated deposition at a rate of 10^{10} atoms/s and with the substrate kept at a temperature of 25 K. Top and bottom panels show, respectively, the system configuration at a certain simulation time, and the corresponding bond angle analysis performed on that configuration (only 12-fold-coordinated Xe atoms are displayed). The color legend in the figure refers to the lower panel only, the color legend for the upper panel is the same as in Fig. 2. Simulation times are as follows: (a) 33 ns, (b) 81 ns, (c) 129 ns, and (d) 201 ns.

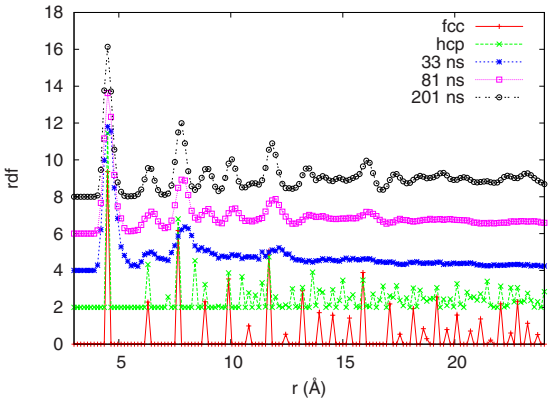

FIG. 9. (Color online) Radial distribution function calculated during a simulated deposition at a rate of 10^{10} atoms/s and with the substrate kept at a temperature of 25 K. The configurations whose radial distribution function is plotted are those shown in (a), (b), and (d) of Fig. 8. Radial distribution function for bulk fcc and hcp crystal structure with the same lattice constant as Xe are also plotted for comparison. The curves are shifted vertically for clarity of display.

out that for both fcc and hcp packing the minimum of energy was achieved when the nearest-neighbor distance was 4.384 Å. Furthermore, fcc packing turned out to be slightly lower in energy for almost all values of lattice constant considered. However, the energy difference between the fcc and the hcp packing was extremely small, ranging from 0.1 up to around 1 meV/atom. The calculated variation in bonding energy per atom as a function of the lattice constant is plotted in Fig. 13(a) for both types of crystal structures considered.

In order to investigate the effect of truncating the potential at a certain distance from the origin, a series of bulk crystal minimizations was undertaken at different cut-off distances. The usual cut-off for the Lennard-Jones potential was at a distance of 2.5σ, where σ was 4.0 Å. In an analogous fashion to before, the cut-off distance was varied between 2.5σ and 6σ, and the structure was minimized locally. Across the whole cut-off distance range investigated, the fcc packing was found to lie lower in energy than the hcp packing, al-

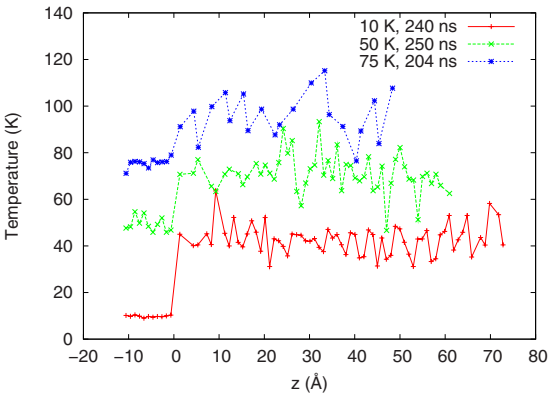

FIG. 10. (Color online) Substrate and deposited species temperature plotted as a function of the vertical z coordinate for growth simulated at three different substrate temperatures. Temperature and time from the beginning of the simulation are indicated in the plot.

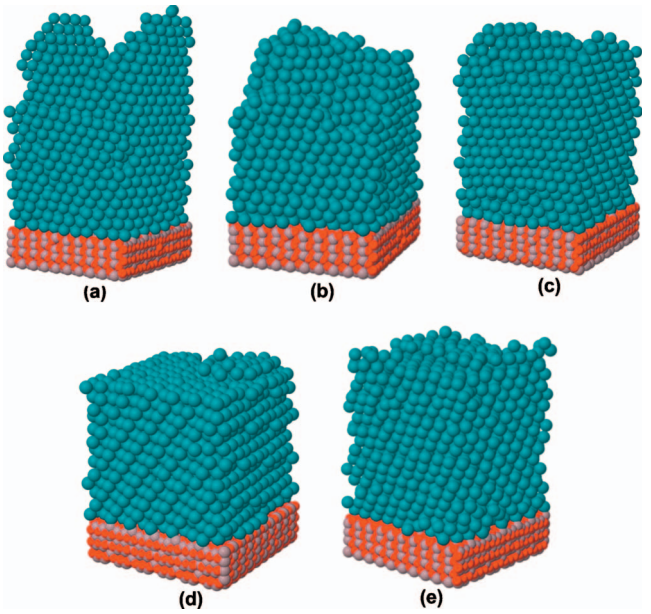

FIG. 11. (Color) Configurations obtained by simulating deposition of Xe at a rate of 10^{10} atoms/s and at different substrate temperatures. Substrate temperatures and simulation times are as follows: (a) 10 K, 240 ns; (b) 25 K, 177 ns; (c) 50 K, 250 ns; (d) 75 K, 204 ns; and (e) 100 K, 210 ns.

though also in this case the difference turned out to be extremely small, ranging from less than 0.1 up to a maximum of around 1 meV/atom [see Fig. 13(b)]. These results thus proved that for this system fcc packing is slightly favored with respect to hcp packing, although the difference in energy between the two crystal structures is extremely tiny. Therefore, competition between fcc-like and hcp-like stacking is to be expected.

B. Single atom diffusion and surface roughness

The roughness of the surface of the deposited species could be tuned by selecting an appropriate substrate temperature. It turned out that the lower the temperature at which the deposition was carried out, the rougher the surface. In general, a nearly perfect layer-by-layer growth was obtained in the approximate temperature range 60–70 K. This was also the range within which fcc crystalline samples with the least number of defects were found to arise as a result of the deposition process (see Sec. III B). These observations are consistent with previous MD studies of homogeneous growth of a model Lennard-Jones system,[9,43,44] where it was found that the best substrate temperature for achieving layer-by-layer growth roughly corresponded to somewhat less than half the system melting temperature.

In order to investigate the reason for different growth modes, calculations of activation barriers to diffusion for a single Xe adatom on a Xe(111) surface were undertaken. We calculated the barriers statically at 0 K; details of the calculation procedure have been given elsewhere.[45,46]

Initially, the activation barrier for thermal self-diffusion on a bare Xe(111) surface was calculated to be equal to 7 meV. This value is in substantial agreement with previous

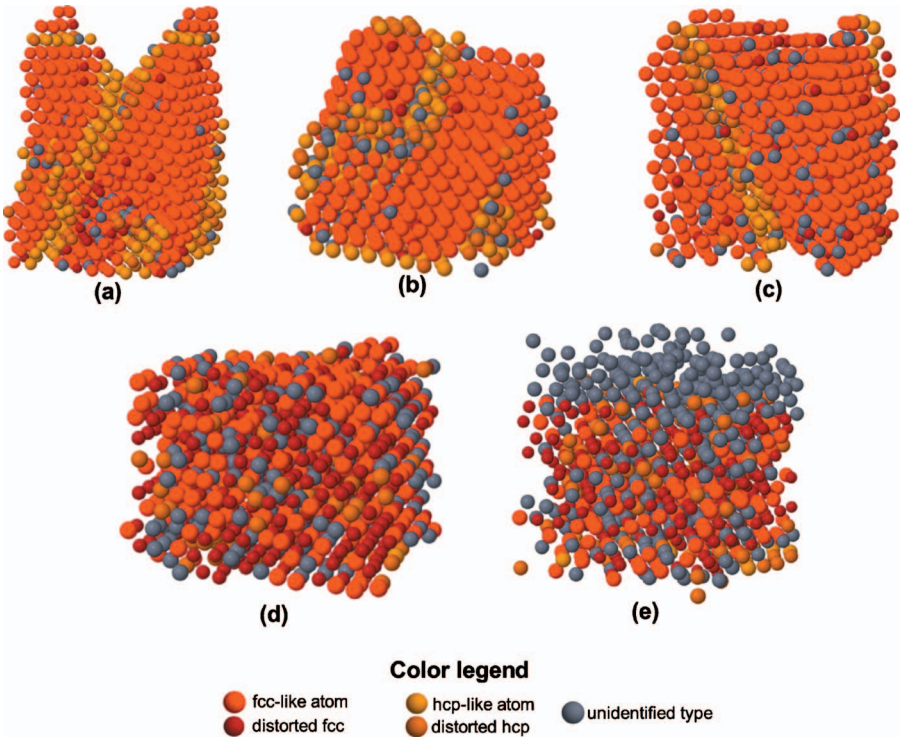

FIG. 12. (Color) Results of bond angle analysis performed on the same structures as shown in Fig. 11. Only 12-fold-coordinated Xe atoms are shown. Substrate temperatures and simulation times are as follows: (a) 10 K, 240 ns; (b) 25 K, 177 ns; (c) 50 K, 250 ns; (d) 75 K, 204 ns; and (e) 100 K, 210 ns.

calculations of self-diffusion on the fcc(111) surface of a Lennard-Jones system.[47] Subsequently, we calculated the barriers for the most important processes whereby an adatom sitting on the upper terrace in proximity to a step edge can diffuse down to the lower terrace. We distinguished between A-type and B-type edge, depending on whether the step exposed a (100) or (111) microfacet on the step riser, respectively.[45] The two processes whose activation barriers were calculated were simple hopping down the step edge and step descent by substitution of an atom previously embedded in the step edge, respectively. The results of the calculations are summarized in Table III.

Hopping down an A- or B-type step is expected to occur with almost the same frequency at all temperatures down to 10 K. However, substitution of an atom on a B step is highly favored with respect to substitution on an A step. The reason for this high discrepancy is the profoundly different transition state assumed by the system during the two processes. In the case of substitution on a B-type step, the step edge atom can follow a minimum energy path, which goes through an intermediate state where it occupies an hcp-type threefold hollow site. On the other hand, in the case of substitution on an A step, the atom which is to be kicked out of the step has to climb a much higher energy barrier since the diffusion path has to go through the on-top position of an underlying atom. This allows substitution on a B-type step to be the most advantageous step descent process for a diffusing adatom among all investigated mechanisms.

If we assume an Arrhenius-type behavior for diffusion, the typical diffusion times can be calculated as a function of temperature as

$$\tau = \frac{1}{\nu_0}\exp\left(\frac{E_d}{k_B T}\right), \tag{3}$$

where E_d is the activation energy to diffusion, k_B is Boltzmann's constant, and ν_0 is the attempt rate, which, by using

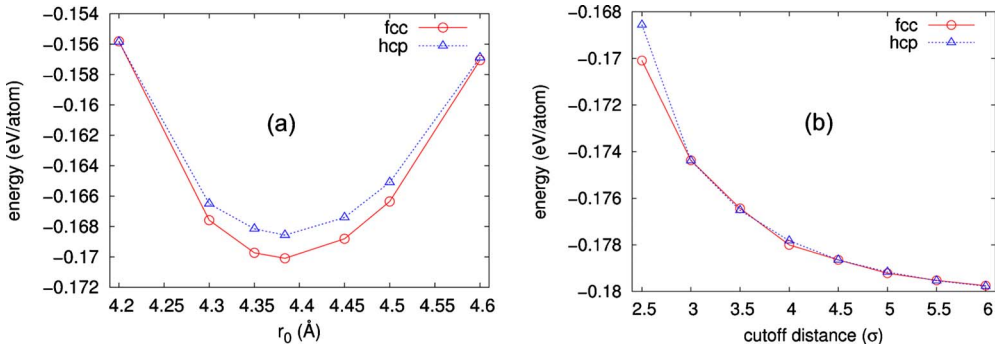

FIG. 13. (Color online) (a) Variation in bonding energy in bulk xenon as a function of the lattice constant for fcc and hcp crystal structure. (b) Variation in bonding energy in bulk xenon as a function of the cut-off distance for the Lennard-Jones potential used. fcc and hcp crystal structure are compared.

TABLE III. Activation energies for diffusion of a single Xe adatom down a step edge on the Xe(111) surface. Energies are expressed in millielectron volt.

	A step	B step
Hopping	34.0	32.8
Substitution	54.9	21.6

transition state theory,[48] can be estimated to be about 10^{12} s^{-1}.

The typical diffusion times calculated by means of Eq. (3) are to be compared with the time interval between the arrival of two consecutive impacting atoms on the surface. With the lower growth rate of 10^{10} atoms/s, processes with typical times on the order of 0.1 ns or lower are allowed to occur in the simulation, whereas slower processes are frozen out. On the basis of Eq. (3), single atom diffusion on the clean surface is a relatively rapid process within the whole interval of temperatures ranging from 10 to 300 K. However, step descent is expected to be seriously frustrated at temperatures below about 50 K.

Therefore, when the growth rate of 10^{10} atoms/s was used in our calculations, simulated deposition below the temperature of 50 K resulted in more or less corrugated surfaces, with lower temperatures favoring three-dimensional growth. For substrate temperatures of about 50 K or higher, mass transport via step descent occurred on a time scale comparable to or smaller than the time interval between two consecutive atom impacts on the surface, thus giving rise to a layer-by-layer growth mode.

This argument was confirmed by our calculations of diffusion of a single Xe adatom on a two-dimensional island on the Xe(111) surface. The adatom was given an initial position at the center of the island and at a distance of 10 Å above it. The initial kinetic energy was the thermal energy at the temperature at which the simulation was carried out. The adatom trajectory was followed for a time span of 4 ns, and the time step of an MD iteration was 2 fs. The interaction among Xe atoms was assumed to be of Lennard-Jones type with the same parameters as in Table II. No step descent within the time span covered in the simulations was observed for temperatures below 50 K. Conversely, in all simulations with a substrate temperature above 50 K the adatom stepped down the edge, at an increasing rate with increasing simulation temperature (see Fig. 14).

These calculations also showed that terrace diffusion can be satisfactorily described as a thermally activated process following the Arrhenius law of Eq. (3) up to temperatures as high as 100 K. One more conclusion one can draw from the results displayed in Fig. 14 is that a Xe adatom diffusing on a close-packed Xe surface is equally likely to occupy a threefold hollow site of fcc and of hcp type. We supported this observation by calculating the difference in adsorption energy between a fcc and a hcp site, which turned out to be 1.6 meV, with the threefold hollow site of fcc type slightly favored with respect to that of hcp type.

We subsequently focused on the impact of a single depositing Xe atom on both the Al_2O_3 surface and the Xe(111)

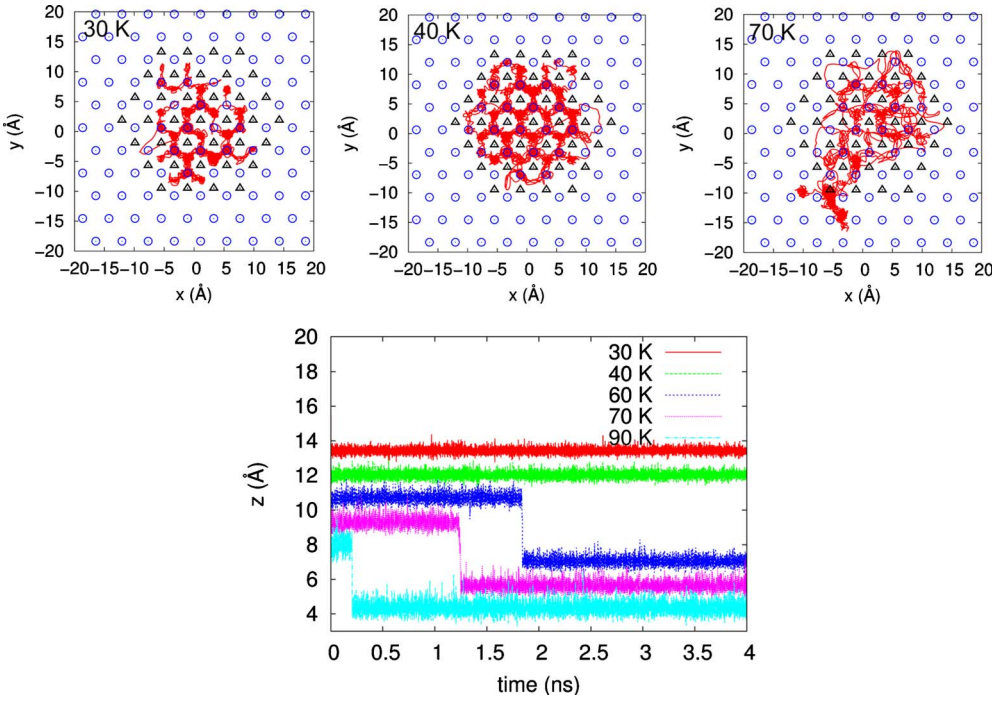

FIG. 14. (Color online) Results of simulations of Xe single adatom diffusion on the Xe(111) surface in the presence of a two-dimensional island. The trajectory of the adatom was followed for a time span of 4 ns. The initial position of the adatom was at the center of the island. The three top panels show the projection of the adatom trajectory on the *xy* plane. The simulation temperature is indicated in each panel. The black triangles and the blue circles mark the position of the adatom in the topmost and lower-lying layer, respectively, at the beginning of the simulation. In the bottom panel the adatom position along the vertical *z* axis is plotted for several temperatures versus the simulation time. The curves are shifted vertically for clarity of display.

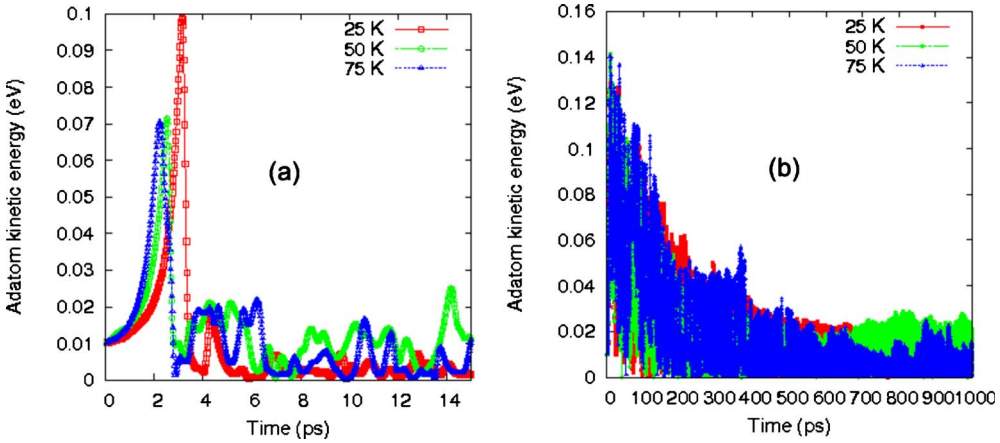

FIG. 15. (Color online) Kinetic energy of a Xe atom impinging (a) on a Xe(111) surface, and (b) on the relaxed Al_2O_3 surface, as a function of time. The impact occurred after approximately between 1.5 and 2.5 ps from the moment when the atom was released. The substrate temperature is also indicated in the plot.

surface. The initial kinetic energy of the adatom was chosen to be equal to 0.01 eV, corresponding to thermal deposition conditions which are to be expected in the experiment. The substrate temperatures investigated varied in the range 10–150 K.

A profoundly different behavior of the impinging adatom was observed depending on the type of the substrate. When single atom deposition was performed on the Xe surface, the adatom was found to gain a substantial amount of kinetic energy due to the attraction exerted by the substrate. Starting from a temperature of approximately 80 K, the adatom reached temperatures as high as 900 K at the moment when it hit the surface. Regardless of the substrate temperature, the adatom lost most of its kinetic energy within a few picoseconds after the impact with the surface, and thermalized to the substrate temperature. The amplitude of the subsequent fluctuations depended on the substrate temperature with wider fluctuations observed for higher substrate temperatures. These observations are in agreement with previous studies of deposition of thin layers of Ag (Ref. 43) and of Pt.[49]

We also studied the impact of a Xe atom deposited on the surface of the optimized Al_2O_3 slab with the same initial kinetic energy as for the deposition on a Xe substrate. The dissipation of the adatom energy in the substrate was much slower than in the case of deposition on the Xe surface. After hitting the surface, the adatom performed a series of bounces of decreasing height and finally thermalized to the substrate temperature after a time span of about 500 ps at all the temperatures investigated. At substrate temperatures as low as 10 K, in some cases the adatom was observed to leave the surface after hitting it. In Fig. 15, the variation in time of the kinetic energy of a Xe adatom deposited on both types of surfaces and at different temperatures is shown for comparison.

These calculations show that the time it took for a Xe adatom impacting on the surface to lose much of its kinetic energy was on the order of a few picoseconds and of 500 ps in the case of impact with a Xe substrate and with an Al_2O_3 substrate, respectively. It can thus be inferred that the time taken for the heat produced by the impact to be dissipated within the bulk crystal was of the same order or higher. Therefore, the time of 5 ps between two consecutive adatom impacts (i.e., impinging rate of 2×10^{11} atoms/s) was far too short for the system to equilibrate to the thermostat temperature. However, when the time between two consecutive adatom impacts was increased to 100 ps (i.e., impinging rate of 10^{10} atoms/s), the extra heat introduced by the adatom impact could flow through the interface between the grown Xe and the substrate and be dissipated due to the action of the thermostat. The slightly higher temperature of the grown Xe with respect to the thermostat temperature can be explained by the incomplete heat transfer between two consecutive atom arrivals.

In this regard, we argue that, during growth, the rate limiting channel for heat dissipation was the heat flow through the interface between the deposited Xe and the substrate. As the results just discussed show, a Xe adatom impacting on the Xe crystal thermalized to the sample temperature in a relatively short time (a few picoseconds). Furthermore, apart from the expected fluctuations, the temperature of the deposited Xe was homogeneous throughout the whole crystal and no obvious temperature gradients in the growth direction could be observed. However, a temperature gap was observed between the Xe crystal and the substrate, thus giving rise to a steep gradient across the interface (see Figs. 3 and 10). Finally, the results reported in Sec. III A 2 confirm that increasing the coupling between the Xe and the substrate surface resulted in a much faster equilibration of the deposited phase to the substrate temperature than in the case of weaker coupling. These arguments allowed us to infer that the heat flow across the interface was the slowest process while establishing thermal equilibrium in the substrate-deposit system.

C. Stacking fault formation

We were interested in casting light on the process of stacking fault formation. By analyzing our calculations of tempering of hot samples grown at a high deposition rate, a hypothesis could be formulated that the stacking faults were

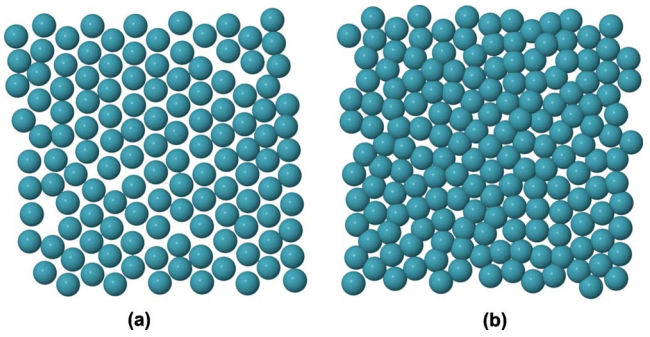

FIG. 16. (Color online) Layer of Xe in closest proximity to the substrate surface. (a) Weak interaction between Xe and Al_2O_3 ($\varepsilon_{Al_2O_3\text{-}Xe}$=0.015 eV); configuration corresponding to Fig. 5(d). (b) Stronger interaction between Xe and Al_2O_3 ($\varepsilon_{Al_2O_3\text{-}Xe}$=0.1 eV); configuration corresponding to Fig. 7(b).

caused by an irregularity in the arrangement of the Xe layer in closest proximity to the substrate surface. Upon closer inspection, the adsorbed Xe layer turned out to be fairly ordered overall, with the average distance between in-plane neighboring atoms close to the nearest-neighbor distance in bulk Xe [see Fig. 16(a)]. We observed that stacking faults originated in general from the interface between the grown sample and the substrate. We verified that the seed for the stacking fault formation was in all cases a row of Xe adatoms adsorbed on the surface which experienced a particularly strong stress field.

When we performed the simulations with the lower strength of interaction between substrate and grown Xe ($\varepsilon_{Al_2O_3\text{-}Xe}$=0.015 eV), we noticed that the Xe atoms in close contact with the substrate tended to arrange themselves as much as possible in a close-packed configuration, although the average in-plane nearest-neighbor distance was slightly larger than in bulk Xe. However, when the interaction between the Xe and the substrate was increased ($\varepsilon_{Al_2O_3\text{-}Xe}$ =0.1 eV), the situation changed. As opposed to the case with the weaker interaction, the first adsorbed layer nucleated in an almost amorphous fashion on top of the substrate surface [see Fig. 16(b)]. This first adlayer acted as a buffer, screening the substrate potential to the layers which nucleated above it. The second nucleated adlayer displayed both amorphous and close-packed regions, whereas the third adlayer was already completely crystalline. In this case there was no obvious seed of the stacking fault, which therefore arose simply as a result of the extremely low energy associated with stacking fault formation.

V. CONCLUSIONS

We modeled the growth of solid Xe from the gas phase on an Al_2O_3 substrate, as it occurs in a real low-temperature atom beam deposition experiment. The process was studied in all its stages, from the dynamics of Xe atoms in the gas phase, over their impact on the surface of the cold substrate and their diffusion on the substrate, to the formation of crystallites and of local and extended defects.

We studied the growth process as a function of synthesis parameters such as the deposition rate and the substrate temperature. Extremely high rates resulted in the formation of amorphous, essentially liquidlike Xe displaying a temperature which was higher than the melting point, due to slow dissipation of the heat of adatom impact on the cold substrate. However, when the grown sample was cooled down to temperatures below 100 K, the establishment of crystalline order in the Xe could be observed. We could distinguish between regions displaying fcc and hcp packing, and we observed a massive presence of stacking faults.

When we simulated growth at a lower rate, we obtained only close-packed crystalline structures. Surface roughness was observed to decrease gradually when the substrate temperature was increased starting from around 10 K. A nearly perfect layer-by-layer growth was achieved for substrate temperatures between 60 and 70 K. These different growth modes could be explained by studying some particularly important diffusion processes of a single Xe atom on a Xe surface. It was found that, for temperatures below 50 K, the diffusion down a step edge occurred at characteristic times which were comparable to, or larger than the time between two consecutive atom arrivals on the surface. This made formation of islands on the terrace and three-dimensional growth much more likely.

Stacking faults were also observed to arise during growth at the lower rate and for substrate temperatures lower than 60 K. We proved that stacking fault formation is very likely for this system by calculating the difference of bonding energy between fcc and hcp packing, which was below 1 meV/atom. Furthermore, we noticed that during diffusion on a close-packed Xe surface, a Xe atom typically spent an equal amount of time in threefold hollow sites of fcc and of hcp type.

Finally, we observed that during growth, and in many cases also during the simulations of tempering of hot Xe samples, the stacking faults originated at the interface between the Xe layers and the substrate. We argued that the origin of these defects was an inhomogeneity in the stress field experienced by the first Xe layer adsorbed onto the substrate surface. We plan to confirm this hypothesis by means of more quantitative investigations. For instance, a method to determine the stress experienced by a microscopic portion of the sample[50–52] could be used to correlate local level pressure and stacking fault formation. If this scenario is confirmed, new perspectives could open up for growing thin and thick solid Xe film displaying arrays of stacking faults whose spatial arrangement could be controlled to one's liking. Moreover, we expect that the method we described above and followed in this work to study the growth of Xe crystals can also be applied to the growth of, e.g., intermetallic or ionic compounds using the low-temperature atom beam deposition method.

ACKNOWLEDGMENTS

N.T. is indebted to Riccardo Ferrando for enlightening discussions and to Roy L. Johnston for carefully proofreading the manuscript. Dieter Fischer's experimental expertise is also gladly acknowledged, along with his willingness to share and discuss his work.

*nico@fkf.mpg.de
†c.schoen@fkf.mpg.de
‡m.jansen@fkf.mpg.de

[1] J. Bernstein, R. J. Davey, and J.-O. Henck, Angew. Chem., Int. Ed. **38**, 3440 (1999).
[2] H. Brune, Surf. Sci. Rep. **31**, 121 (1998).
[3] F. Rosei and R. Rosei, Surf. Sci. **500**, 395 (2002).
[4] E. Vlieg, Surf. Sci. **500**, 458 (2002).
[5] A. C. Levi and K. Kotrla, J. Phys.: Condens. Matter **9**, 299 (1997).
[6] H. Jónsson, Annu. Rev. Phys. Chem. **51**, 623 (2000).
[7] M. Schneider, A. Rahman, and I. K. Schuller, Phys. Rev. B **34**, 1802 (1986).
[8] E. T. Gawlinski and J. D. Gunton, Phys. Rev. B **36**, 4774 (1987).
[9] S. M. Paik and S. Das Sarma, Phys. Rev. B **39**, 1224 (1989).
[10] W. D. Luedtke and U. Landman, Phys. Rev. B **40**, 11733 (1989).
[11] I. Kwon, R. Biswas, G. S. Grest, and C. M. Soukoulis, Phys. Rev. B **41**, 3678 (1990).
[12] P. Guan, D. R. Mckenzie, and B. A. Pailthorpe, J. Phys.: Condens. Matter **8**, 8753 (1996).
[13] N. C. Hernández and J. F. Sanz, J. Phys. Chem. B **105**, 12111 (2001).
[14] M. Mungan, Y. Weisskopf, and M. Erbudak, Phys. Rev. B **76**, 195443 (2007).
[15] J. R. Arthur, Surf. Sci. **500**, 189 (2002).
[16] D. Fischer and M. Jansen, J. Am. Chem. Soc. **124**, 3488 (2002).
[17] D. Fischer and M. Jansen, Angew. Chem., Int. Ed. **41**, 1755 (2002).
[18] D. Fischer, Z. Cancarevic, J. C. Schön, and M. Jansen, Z. Anorg. Allg. Chem. **630**, 156 (2004).
[19] Y. Liebold-Ribeiro, D. Fischer, and M. Jansen, Angew. Chem., Int. Ed. **47**, 4428 (2008).
[20] D. Fischer (private communication). The experiment was carried out in a vacuum chamber where the base pressure was 1×10^{-8} mbar. The substrate was a single-crystal sapphire with (0001) orientation epitaxially polished. The Xe gas was introduced into the chamber at a rate of approximately 0.5 cm^3/min and the chamber pressure during deposition was 2×10^{-5} mbar, or lower. The substrate was cooled down to a temperature range of 20–60 K and the deposition process typically continued for a few hours, resulting in films of about 100 nm thickness. X-ray diffraction patterns of the grown samples were measured at different substrate temperatures, indicating the simultaneous presence of regions with fcc and hcp packing of Xe atoms.
[21] T. Welker and T. P. Martin, J. Chem. Phys. **70**, 5683 (1979).
[22] V. A. Bracken, P. Gürtler, and J. G. McCaffrey, J. Chem. Phys. **107**, 5290 (1997).
[23] L. Huang, S. J. Chey, and J. H. Weaver, Phys. Rev. Lett. **80**, 4095 (1998).
[24] J. S. Palmer, P. Swaminathan, S. Babar, and J. H. Weaver, Phys. Rev. B **77**, 195422 (2008).
[25] D. Frenkel and B. Smit, *Understanding Molecular Simulation: From Algorithms to Applications* (Academic Press, San Diego, 1996).
[26] M. Matsui, Phys. Chem. Miner. **23**, 345 (1990).
[27] R. Ahuja, A. B. Belonoshko, and B. Johansson, Phys. Rev. E **57**, 1673 (1998).
[28] G. Gutiérrez, A. B. Belonoshko, R. Ahuja, and B. Johansson, Phys. Rev. E **61**, 2723 (2000).
[29] D. Wolf, P. Keblinski, S. R. Phillpot, and J. Eggebracht, J. Chem. Phys. **110**, 8254 (1999).
[30] W. Hogervorst, Physica (Utrecht) **51**, 77 (1971).
[31] A. A. Clifford, P. Gray, and N. Platts, J. Chem. Soc., Faraday Trans. 1 **73**, 381 (1977).
[32] G. Vidali, G. Ihm, H.-Y. Kim, and M. W. Cole, Surf. Sci. Rep. **12**, 135 (1991).
[33] S. Blonski and S. H. Garofalini, Surf. Sci. **295**, 263 (1993).
[34] H. C. Andersen, J. Chem. Phys. **72**, 2384 (1980).
[35] J. Julin, I. Napari, and H. Vehkamäki, J. Phys. Chem. **126**, 224517 (2007).
[36] E. Kelly, M. Seth, and T. Ziegler, J. Phys. Chem. A **108**, 2167 (2004).
[37] P. J. Steinhardt, D. R. Nelson, and M. Ronchetti, Phys. Rev. B **28**, 784 (1983).
[38] J. D. Honeycutt and C. Andersen, J. Phys. Chem. **91**, 4950 (1987).
[39] J. Yang, H. Gould, and W. Klein, J. Chem. Phys. **93**, 711 (1990).
[40] P. Rein ten Wolde, M. J. Ruiz-Montero, and D. Frenkel, J. Chem. Phys. **104**, 9932 (1996).
[41] J. R. Morris, Phys. Rev. B **66**, 144104 (2002).
[42] L. J. Peng, J. R. Morris, and Y. C. Lo, Phys. Rev. B **78**, 012201 (2008).
[43] C. M. Gilmore and J. A. Sprague, Phys. Rev. B **44**, 8950 (1991).
[44] M. Schneider, A. Rahman, and I. K. Schuller, Phys. Rev. Lett. **55**, 604 (1985).
[45] R. Ferrando and G. Tréglia, Phys. Rev. B **50**, 12104 (1994).
[46] N. Totò, R. Ferrando, Q. Guo, and R. L. Johnston, Phys. Rev. B **75**, 195434 (2007).
[47] J. Johansson and S. Toxvaerd, Phys. Rev. B **69**, 233401 (2004).
[48] P. Hänggi, P. Talkner, and M. Borkovec, Rev. Mod. Phys. **62**, 251 (1990).
[49] D. Adamović, V. Chirita, E. P. Münger, L. Hultman, and J. E. Greene, Phys. Rev. B **76**, 115418 (2007).
[50] D. H. Tsai, J. Chem. Phys. **70**, 1375 (1979).
[51] V. Vitek and T. Egami, Phys. Status Solidi B **144**, 145 (1987).
[52] P. C. Kelires and J. Tersoff, Phys. Rev. Lett. **63**, 1164 (1989).